POTENTIAL VORTICITY

Roger K. Smith

March 3, 2003

Contents

1 Potential Vorticity Thinking - How might it help the forecaster? 2

1.1 Introduction 2
1.2 What is PV-thinking? 4
1.3 Examples of 'PV-thinking' 7
1.3.1 A thought-experiment for understanding tropical cyclone motion 7
1.3.2 Kelvin-Helmholtz shear instability 9
1.3.3 Rossby wave propagation in a β-plane channel 12
1.4 The structure of EPV in the atmosphere 13
1.4.1 Isentropic potential vorticity maps 14
1.4.2 The vertical structure of upper-air PV anomalies . . . 18

2 A Potential Vorticity view of cyclogenesis 21

2.1 Preliminary Ideas 21
2.2 Surface layers of PV 21
2.3 Potential vorticity gradient waves 23
2.4 Baroclinic Instability 28
2.5 Applications to understanding cyclogenesis 30

3 Invertibility, iso-PV charts, diabatic and frictional effects. 33

3.1 Invertibility of EPV 33
3.2 Iso-PV charts 33
3.3 Diabatic and frictional effects 34
3.4 The effects of diabatic heating on cyclogenesis 36
3.5 The demise of cutoff lows and blocking anticyclones 36
3.6 Advantage of PV analysis of cutoff lows 37
3.7 The PV structure of tropical cyclones 37

Chapter 1

Potential Vorticity Thinking - How might it help the forecaster?

1.1 Introduction

A review paper on the applications of Potential Vorticity (PV-) concepts by Brian Hoskins, Michael McIntyre and Andy Robertson in the Quarterly Journal of the Royal Meteorological Society in October 1985 (Hoskins *et al.*, 1985; henceforth referred to as HMR) led to a dramatic increase in their use for understanding dynamical processes in meteorology, at least at the research level. In my experience, these ideas have not filtered through to the forecasting 'bench', perhaps for one good reason; until recently forecasters have not had access to PV charts! With the proliferation of diagnostic aids in forecasting offices throughout Australia, this obstacle has now be removed. It remains only to persuade the forecaster that PV concepts have something to offer by way of understanding and I view this as a challenge for the researcher.

Potential vorticity concepts are not new, they have their origins in the work of Rossby and Ertel in the early 40's and their utility was recognized in a series of visionary papers by Kleinschmidt in the early 50's. A comprehensive historical survey is given in HMR. Recent developments have gone a long way, *inter alia*, to bridge the gap between early baroclinic instability theories of cyclogenesis and observations. Following the pioneering studies by Charney (1947) and Eady (1949), much of the early theoretical work on baroclinic instability was concerned with the evolution and structure of small amplitude perturbations to a baroclinic zonal shear flow. On the other hand, cyclogenesis is observed to occur in conjunction with finite amplitude dis-

turbances within a zonally nonuniform flow. Even so, baroclinic instability theory does predict many of the observed features of real cyclones including the scale, growth rate, and wave structure (e.g. pressure trough sloping westward with height).

While baroclinic instability theory may be perceived by forecasters as a rather esoteric pursuit, a group of closely related ideas on the"steering" and "development" of extratropical cyclones, involving popular jargon such as "PVA-maxima", do enjoy a prominent place. These ideas go back to a remarkably insightful and practically-orientated paper by Sutcliffe (1947) on "The theory of development". Sutcliffe's theory, based on quasi-geostrophic dynamics, provides a dynamical basis for a few important forecasting rules. These include the thermal steering principle, which states that extratropical cyclones tend to move with the speed of and in the direction of the 1000-500 mb thermal wind, as well as criteria for the development and nondevelopment of cyclones in terms of the position of the surface low in relation to the thermal trough (or more or less equivalently to that at 500 mb). Indeed, Sutcliffe's theory is one of the few to provide practical rules with a sound dynamical basis that can be applied 'on the bench'. However, like any theory it has limitations and in my experience, the ideas are frequently 'stretched' by forecasters; i.e., they are often used to construct arguments or to justify scenarios in circumstances in which the theory is not really valid. Frequently an important misconception is that the theory is a predictive one; in reality it is no more than a diagnostic one for the tendencies at a particular instant of time. Moreover the theory is often used to construct 'cause and effect' arguments when, in fact, it reflects only one aspect of the dynamics of cyclogenesis - it considers only the initial tendencies of the surface low (direction, speed, deepening, filling etc.), but does not take into account the mutual evolution of the complete system (surface low + thermal trough/ridge etc.). I do not have time here to go into details: a more complete discussion of Sutcliffe's theory of development, its strong points and limitations are to be found in Chapter 10 of my Lecture Notes on Dynamical Meteorology (Smith, 1998)[1].

For reasons just outlined, Sutcliffe's theory cannot hope to out perform even the most basic two-layer baroclinic numerical forecast model and it is not surprising that with the relatively sophisticated and normally reliable numerical products currently available, there would need to be very compelling reasons for a forecaster to ignore the numerical products in favour of

[1]A pdf file of these notes may be downloaded from the website: http://www.meteo.physik.uni-muenchen.de. Please email me at roger@meteo.physik.uni-muenchen.de for the precise location and to obtain a password.

Sutcliffe's rules. Nevertheless, to quote Davis and Emanuel (1991), " ... a proper integration of the equations of motion is not synonymous with a conceptual grasp of the phenomena being predicted". The forecaster would like to have not only the numerical prognoses, but a modern conceptual framework in which to interpret them. This is where "PV-thinking" can help and my ambitious aim in this article is to show how.

1.2 What is PV-thinking?

There are two main approaches to the solution of fluid flow problems:

1. We can integrate the momentum, continuity and thermodynamic equations (the so-called primitive equations) directly, or

2. In certain cases we can use the vorticity-streamfunction formulation as described below.

The former method may provide rather less insight into the dynamics of a particular phenomenon than the latter, partly because we cannot arbitrarily specify the force field (i.e. the pressure gradient field) in a fluid (see my article "Understanding fluid motion", Smith 2003). In contrast, the vorticity-streamfunction approach can provide a neat conceptual framework in which to 'understand' the dynamics. I shall illustrate what I mean in section 1.3 by some very simple examples. First I should like to show how the formulation goes in a series of flow systems of increasing complexity.

For a homogeneous (uniform density) two-dimensional nonrotating flow, the vorticity-streamfunction approach is particularly insightful. Then the vorticity ζ normal to the plane of motion is materially conserved (i.e. following fluid parcels). Expressed mathematically,

$$\frac{D\zeta}{Dt} = 0, \tag{1.1}$$

where $\zeta = v_x - u_y$ is the vorticity, u and v are the velocity components in the x and y directions, and $D/Dt = \partial/\partial t + \mathbf{u}\cdot\nabla$ is the material derivative, where t is the time and $\mathbf{u} = (u, v)$. The continuity equation implies the existence of a streamfunction ψ for which

$$u = -\psi_y, \ v = \psi_x, \tag{1.2}$$

and then

$$\nabla^2\psi = \zeta. \tag{1.3}$$

The latter is an elliptic[2] partial differential equation, a so-called Poisson equation, which may be solved diagnostically (i.e. at a particular instant of time) for ψ, given the distribution of vorticity ζ throughout the domain at this time, together with suitable boundary conditions along the entire boundary of the flow domain. In this formulation, Eq.(1.1), written in the form $\partial\zeta/\partial t = -\mathbf{u}\cdot\nabla\zeta$, is used to update the vorticity field at a new time level and Eq.(1.3) is used to diagnose the corresponding flow pattern. Following HMR we refer to equations such as (1.3) as 'invertibility' relations or principles, i.e. a knowledge of ζ can be *inverted* to give a knowledge of ψ and hence, using (1.2), a complete knowledge of the flow.

For a rotating fluid on an f-plane[3] or β-plane, Eq.(1.1) must be replaced with

$$\frac{D}{Dt}(\zeta + f) = 0, \tag{1.4}$$

expressing the conservation of absolute vorticity $f + \zeta$. However, Eq. (1.3) remains valid as the invertibility relation. I shall give some examples showing the power of arguments based on (1.4) and (1.3) in section 1.3, but for the moment let us continue.

For a divergent flow having variable depth $h(x, y, t)$, Eq.(1.4) must be replaced with

$$\frac{D}{Dt}\left[\frac{\zeta + f}{h}\right] = 0, \tag{1.5}$$

expressing the conservation of *potential vorticity for a homogeneous layer of fluid*. In this case, the continuity equation is

$$\frac{Dh}{Dt} = -h\nabla\cdot\mathbf{u}, \tag{1.6}$$

and unlike the nondivergent cases it does not provide a diagnostic equation relating the flow field to the PV distribution unless some sort of balance is assumed. For example if the motion is assumed to be quasi-geostrophic (implying a restriction on the degree to which h may vary and therefore on the magnitude of the divergence), (1.6) can be approximated by $\nabla\cdot\mathbf{u} = 0$, whereupon Eq.(1.3) again provides a valid invertibility relation. For three-

[2]Elliptic equations are a particular type of partial differential equation that arise naturally in equilibrium problems, such as the problem for equilibrium displacement of a stretched membrane subjected to a (steady) prescribed force distribution. See e.g. Fig. 1.2

[3]Of course, on an f-plane, (1.4) reduces to (1.1)

dimensional, quasi-geostrophic motion of a rotating stratified fluid, the prognostic equation is for the quasi-geostrophic PV, or pseudo-PV (PPV), q, i.e.,

$$\frac{Dq}{Dt} = 0, \tag{1.7}$$

where

$$\nabla_h^2 \psi + f + \varepsilon \frac{\partial^2 \psi}{\partial z^2} = q. \tag{1.8}$$

Here $\varepsilon = f^2/N^2$, N being the Brunt-Väisälä frequency[4], assumed here to be a constant for simplicity. Equation (1.8) is again an elliptic differential equation relating ψ diagnostically to q, given suitable boundary conditions on the former.

For the general adiabatic motion of a rotating stratified fluid, a quantity P called the Ertel potential vorticity (EPV) is conserved, i.e.,

$$\frac{DP}{Dt} = 0, \tag{1.9}$$

where

$$P = \frac{(\boldsymbol{\omega} + \mathbf{f}) \cdot \nabla \theta}{\rho}, \tag{1.10}$$

being the full vector vorticity (= curl $\mathbf{u}$) and ρ the fluid density. When expressed in isentropic coordinates, P takes the particularly simple form

$$P = -g(\zeta_\theta + f)(\partial \theta / \partial p), \tag{1.11}$$

where ζ_θ is the "vertical" component of relative vorticity in isentropic coordinates and p is the pressure (here "vertical" means normal to an isentropic surface). Now the scalar product no longer appears. Moreover, the vertical advection in the derivative D/Dt is identically zero also. Then (1.9) says that P is conserved on isentropic surfaces. This turns out to be a very useful result and later we shall discuss isentropic charts of EPV for the atmosphere[5].

Unfortunately, as in the case of a divergent homogeneous flow with variable depth as discussed above, there is no unique relationship between the flow field and the EPV distribution, unless we make also some sort of balance assumption (e.g. geostrophic balance, gradient-wind balance or some

[4] N is defined by the formula $N^2 = (g/\theta)(\partial\theta/\partial z)$, where z is the height, θ is the potential temperature and g is the acceleration due to gravity.

[5] Note, HMR use the term IPV for P, an acronym for isentropic potential vorticity. This acronym has since been dropped as EPV is just as valid in other coordinate systems.

other form of nonlinear balance). As it turns out, this is not such a major restriction and we can construct arguments for quite realistic atmospheric flows based on the EPV structure and its evolution in much the same way as in the simple examples to be discussed now.

1.3 Examples of 'PV-thinking'

To answer the question posed in section 1.2, I shall apply 'PV-thinking' to three simple two-dimensional flows, the first and third governed by (1.4) and (1.3), the second by (1.1) and (1.3).

1.3.1 A thought-experiment for understanding tropical cyclone motion

Perhaps the simplest problem in the theory of tropical cyclone motion considers the translation of an initially symmetric vortex on a β-plane at rest (Fig. 1.1(a)). Numerical experiments have shown that for a vortex in the Southern Hemisphere, the subsequent motion is towards the southwest; in the northern hemisphere it is towards the northwest. We assume the motion to be barotropic and nondivergent so that the PV (in this case the absolute vorticity $f + \zeta$) is conserved.

As time proceeds, air parcels on the eastern side of the vortex move poleward, conserving their initial $f + \zeta$. Since f becomes increasingly more negative (i.e. cyclonic), ζ increases and becomes more anticyclonic. Equatorward motion on the western side of the vortex leads to a cyclonic tendency in relative vorticity and the net result is the development of a dipole asymmetry in the vorticity field (Fig. 1.1(b)). Because of advection by the basic vortex motion, this asymmetry does not remain oriented west-east, but rotates cyclonically as shown. Since the symmetric vortex cannot advect itself, the subsequent motion must be attributed to the flow field associated with the vorticity asymmetry which has a southwestward component across the vortex centre (northwestward in the Northern Hemisphere). For a full discussion of this problem and a simple analytic solution for the dipole vorticity asymmetry I refer you to recent papers by Smith *et al.* (1990) and Ulrich and Smith (1991). The latter paper gives an analytic solution for the inversion problem, i.e. given the asymmetric vorticity distribution ζ_a, what is the corresponding streamfunction ψ_a satisfying appropriate boundary conditions?

In the foregoing problem, I appealed to your intuition when deducing the flow field between the asymmetric vorticity dipole which satisfies $\nabla^2 \psi_a = \zeta_a$ although I show the calculated field in Fig. 1.1(c) for completeness. Now,

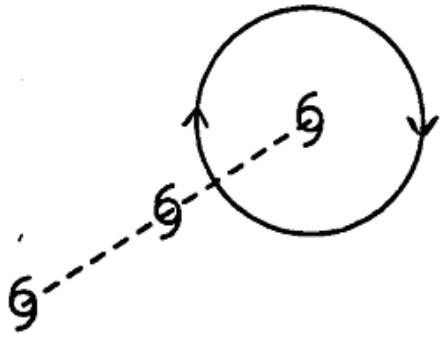

(a)

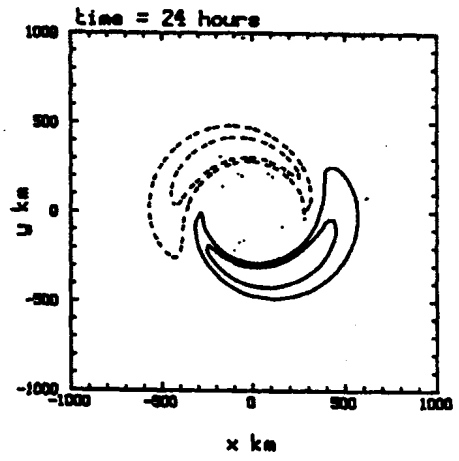

(b)

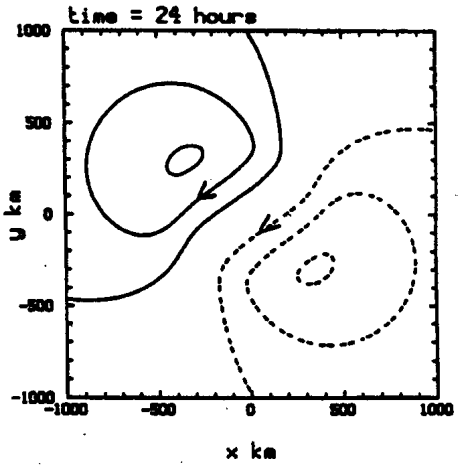

(c)

Figure 1.1: Flow configuration on a Southern Hemisphere β-plane depicting the simplest thought experiment in the theory of tropical cyclone motion, i.e. the motion of an initially symmetric vortex in the case of zero basic flow. The dashed line in panel (a) denotes the vortex track towards the south-west. (b) Shows the pattern of the vorticity asymmetry ζ_a, that develops after 24 hours (adapted from Smith and Ulrich, 1990). (c) Shows the asymmetric streamfunction pattern corresponding with ζ_a obtained analytically by solving $\nabla^2\psi_a = \zeta_a$. Negative contours are dashed. Contour intervals are arbitrary.

I would like to show how we use our intuition more generally. Consider a flexible membrane with uniform properties stretched across a wire frame and subject to a steady force distribution $F(x, y)$ as shown in Fig. 1.2.

I have shown the case where the wire frame has the form of a rectangle and lies in the plane $z = 0$. It happens that the equilibrium distribution of the membrane displacement $\xi(x, y)$ satisfies the equation

$$\nabla^2 \xi = -F, \tag{1.12}$$

subject to the boundary condition $\xi = 0$ on the boundary of the domain (i.e. along the wire frame). Therefore, we may use our intuition to infer qualitatively the structure of the membrane displacement (i.e. if the force is positive over a region, the membrane displacement will be positive). This problem provides a convenient analogy to deduce qualitatively the structure of solutions to the invertibility equation $\nabla^2 \psi = \zeta$, given the vorticity distribution. We simple interpret ζ as *minus the force* on the membrane and ψ as the membrane displacement. Thus regions of positive vorticity tend to be associated with areas of negative streamfunction and vice versa. However, because the inversion is a global problem, i.e., the membrane is under tension, extrema in the vorticity field are not necessarily collocated with extrema in the streamfunction pattern (compare for example Fig. 1.1(b) with Fig. 1.1(c)). A slight reformulation of the membrane problem allows us to handle other types of boundary conditions on ψ (see Smith, 1998, Appendix to Chapter 14 for details).

1.3.2 Kelvin-Helmholtz shear instability

Many cases of clear air turbulence are thought to be associated with a form of shear instability when the vertical wind shear in a stably stratified layer of air is large. An idealized model for shear instability is to consider two parallel homogeneous airstreams with uniform velocities U_1 and U_2 (Fig. 1.3). We consider here only the case of weak stratification and neglect the density difference between the airstreams. In this model the shear is all concentrated at the interface between the airstreams, which can be thought of as an infinitesimally thin sheet of horizontally-oriented vorticity. We can use vorticity arguments to understand why this flow is unstable. We suppose that the vortex sheet is perturbed by a sinusoidal wave-like disturbance as shown in Fig. 1.3. We explore then the subsequent evolution of the vorticity field, which in this case is governed by Eq. (1.1) (now we take x horizontal and y vertical). Consider a material particle at the point B where the vertical displacement is a maximum. The motion at this point is due to the influence

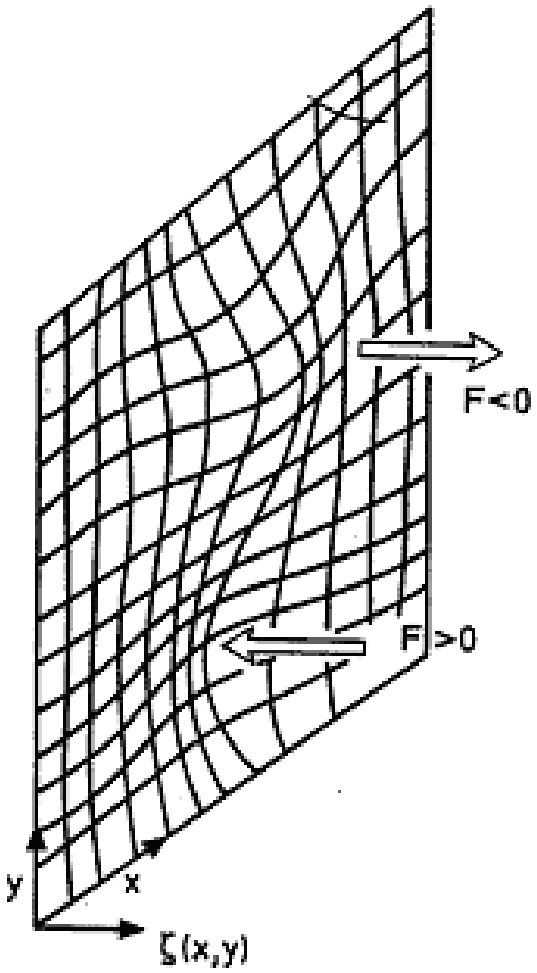

Figure 1.2: Equilibrium displacement $\xi(x, y)$ of a stretched membrane over a square frame under the force distribution $F(x, y)$. Intuition about how a membrane responds provides a means of deducing the qualitative structure of solutions to Poisson's equation.

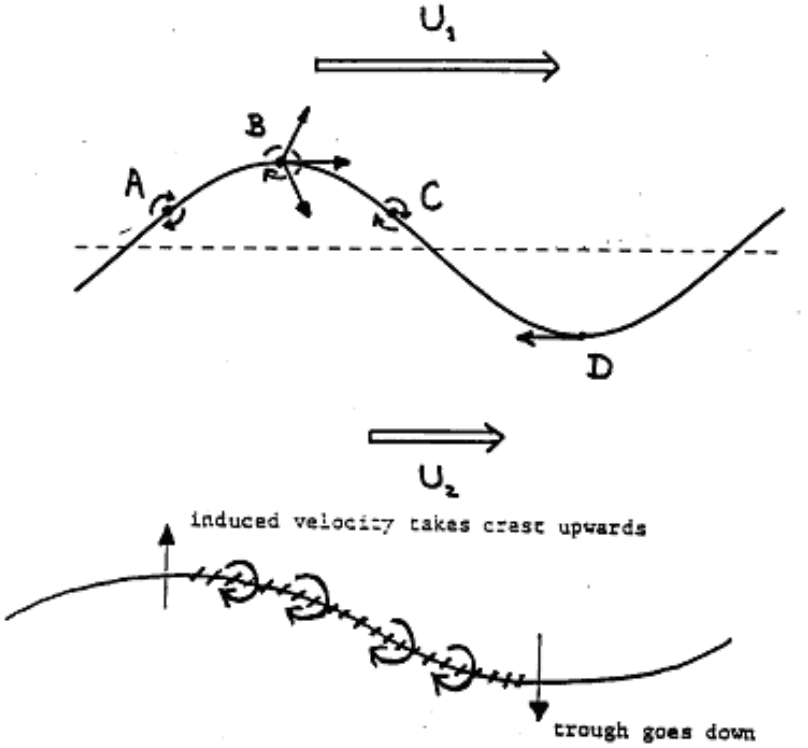

Figure 1.3: Interpretation of Helmholtz shear instability in terms of the self-induced amplification of a distorted vortex sheet (see text for discussion).

of the vorticity distribution at all other points. For example, vortex elements at the points A and C, symmetrically placed with respect to B, induce velocity contributions as shown. The net effect gives zero component in the y-direction, but there is a net horizontal component towards C. The total contribution summed over all symmetrically placed points has a similar structure. For the parcel with maximum negative displacement at D, there is a net induced motion also towards C. At first then, the vorticity in the sheet tends to clump to towards regions such as between B and D, i.e. the vortex sheet breaks up into isolated centres of vorticity (lower panel in Fig. 1.3). As this occurs the initial symmetry of the vorticity distribution about B and D is broken and the induced velocity at these points is such as to increase their lateral displacement. This is a run-away process unless suitably modified by nonlinearities as the displacement amplitude becomes large. In this example we applied the invertibility principle without direct reference to the solution of (1.3), but the arguments are equivalent.

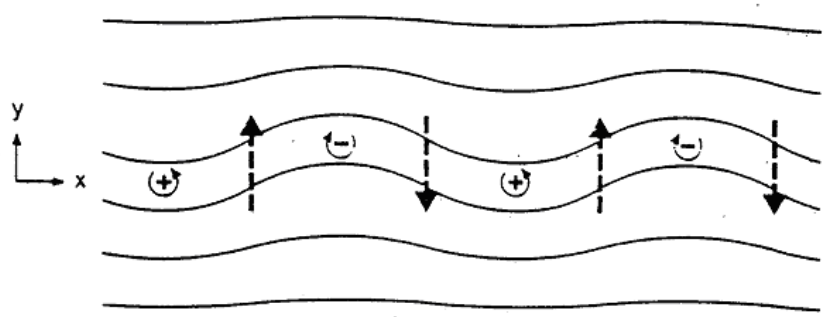

Figure 1.4: Sketch of the absolute vorticity contours $\zeta + f =$ constant (solid lines) for a sinusoidal anomaly pattern along a band of latitudes in a β-plane channel. Shown also is the induced velocity field. These patterns are characteristic of a simple Rossby wave.

1.3.3 Rossby wave propagation in a β-plane channel

Our third example provides an interpretation of Rossby (or planetary) wave dynamics on a middle latitude β-plane channel (Fig. 1.4) as discussed by McIntyre (1988a).

We assume that the channel has rigid boundaries at latitudes corresponding with specific values of y. The basic state is assumed to be one of relative rest ($\psi = 0$ everywhere) and f has a uniform y-gradient ($\beta > 0$) . Then the absolute vorticity contours of the basic state $q = f_0 + \beta y =$ constant lie along latitude circles. Because the ensuing motion conserves the absolute vorticity $q = \zeta + f$, the contours of q remain material contours. If a disturbance makes these contours undulate sinusoidally as shown in Fig. 1.4, the perturbation $q = (= q - \overline{q})$ will vary sinusoidally also, having alternatively positive and negative sign as indicated in the figure. To see what the induced ψ field must look like we can think of the ζ pattern as corresponding with the force on an elastic membrane that is pushed and pulled alternatively in the same pattern. The sides of the membrane are held down with zero displacement along lines corresponding with the channel boundaries. According to our membrane analogy, the ψ field will have a similar pattern to the ζ field, but with opposite sign. Thus ψ will have hills and valleys centred respectively on the minus and plus signs, and the strongest north-south winds will occur at intermediate positions, a quarter of a wavelength out of phase with the displacement, and in the sense shown by the heavy, dashed arrows in the figure (recall that $v = \partial\psi/\partial x$). It is easy to see what this induced velocity

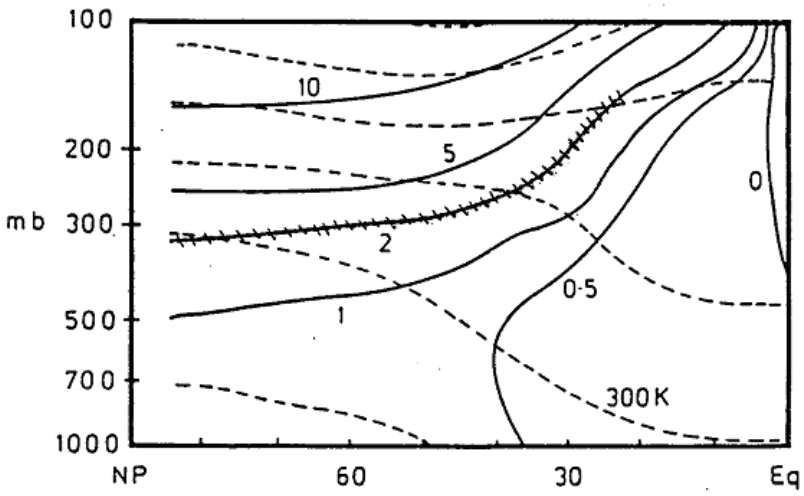

Figure 1.5: The climatological P and q distribution below 100 mb in the Northern Hemisphere winter. The dashed contours are those of q, drawn every 30 K. Values of P are given in terms of the unit PVU = 10^{-6} m^2 kg s^{-1}, and contours are drawn at 0, 0.5, 1, 2, 5 and 10. The "dynamical" tropopause, specified by 2 PVU, is indicated by stippling (from Hoskins, 1990).

field will do to the material contours: it is clear that the undulations will propagate westward. The motions are stable (or to be more precise, neutrally stable) because the velocity perturbation is zero where the displacements of particles from their equilibrium positions are a maximum.

In each of these examples, the line of argument is the same. First we infer the vorticity distribution implied by the conservation property (1.1) or (1.4). Then we invoke the invertibility principle (1.3) to infer the flow field associated with this distribution. In general, the induced flow is associated with *anomalies* of vorticity.

1.4 The structure of EPV in the atmosphere

Before considering how the foregoing ideas can be extended to the atmosphere, we examine the mean structure of EPV in the atmosphere as well as its day-to-day variation. Figure 1.5 shows the climatological distribution of P and the potential temperature θ, zonally-averaged, for the Northern Hemisphere winter. From the pole to about 25° latitude, the $P = 2$ surface corresponds to the tropopause (the units of P are 10^{-6} km^2 kg^{-1} s^{-1},

commonly referred to as 1 PV-unit (or 1 PVU). Tropospheric values of PV are typically less than 1.5 PVU and vertical gradients thereof are associated mainly with the variation of ρ with height. An almost discontinuous jump occurs at the tropopause because of the jump in static stability, characterized by $-\partial\theta/\partial p$, across the tropopause. Stratospheric values of PV generally exceed 4 PVU. At latitudes equatorward of about 25°, PV values decrease with the decline in $f + \zeta$ as the equator is approached. In this region, PV surfaces slope steeply upwards towards the equator.

The typical variation of PV along isentropic surfaces can be readily inferred from Fig. 1.5. For example, along the 300 K isentrope, which lies mainly in the troposphere, PV gradients are generally small. On the other hand, the 330 K isentrope samples stratospheric air in higher latitudes and middle tropospheric air at low latitudes. PV values and gradients are relatively small equatorwards of where this surface meets the tropopause and relatively large polewards. The 360 K isentrope samples mostly stratospheric air, except at times in very low latitudes.

1.4.1 Isentropic potential vorticity maps

HMR show Northern Hemisphere contour plots of PV on selected isentropic surfaces for a particular synoptic situation and compare features on these with those on more conventional charts. For example they showed that important features in isobaric charts of geopotential height, such as troughs, ridges, cut off lows and blocking anticyclones correspond with distinctive features on isentropic maps of PV. An extract from their Fig. 1.2 is shown in Figs. 1.6 and 1.7.

As expected from the discussion above, PV gradients are large in a region encircling the pole, where the particular isentropic surface lies in the stratosphere (surfaces 350 K and 330 K are shown in the figure), but are weak where it lies further equatorwards in the troposphere. The tropopause, which is marked approximately by the blackened region in Figs. 1.6 and 1.7b, is noticeably contorted and there are small regions where high PV air is totally encircled by low PV air and vice versa. These features may be associated with cut-off lows and blocking anticyclones, respectively, in the geopotential fields. In other places, long tongues of high PV air extrude from the stratospheric "reservoir" and tongues of low PV air intrude polewards into the region normally occupied by stratospheric air on the particular isentrope. These regions tend to be associated respectively with the troughs and ridges on isobaric charts. Specific features are marked in Figs. 1.6 and 1.7. Feature A is primarily an upper level feature and corresponds with an upper tropospheric low while B is associated with an upper level trough.

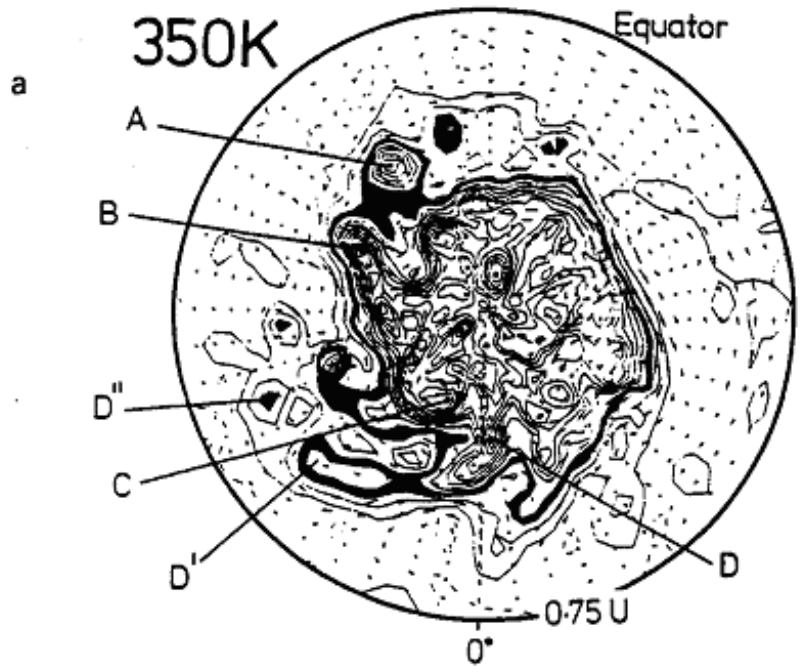

Figure 1.6: Northern Hemisphere PV maps on the 350 K isentropic surface 30 September 1982. The contour intervals is 0.75 PVU. The values 2.25-3 PVU have been blacked in. Also shown are arrows indicating the horizontal component of the velocity vector on these isentropic surfaces. The points of the arrowheads are plotted at the mid-points of the arrows which also mark the grid-points to which the vectors refer. An arrow length from the 40°-60° latitudinal circles would indicate a speed of 100 ms^{-1}. The boundary circle is the equator. The lettering denotes features referred to in the text. (from HMR)

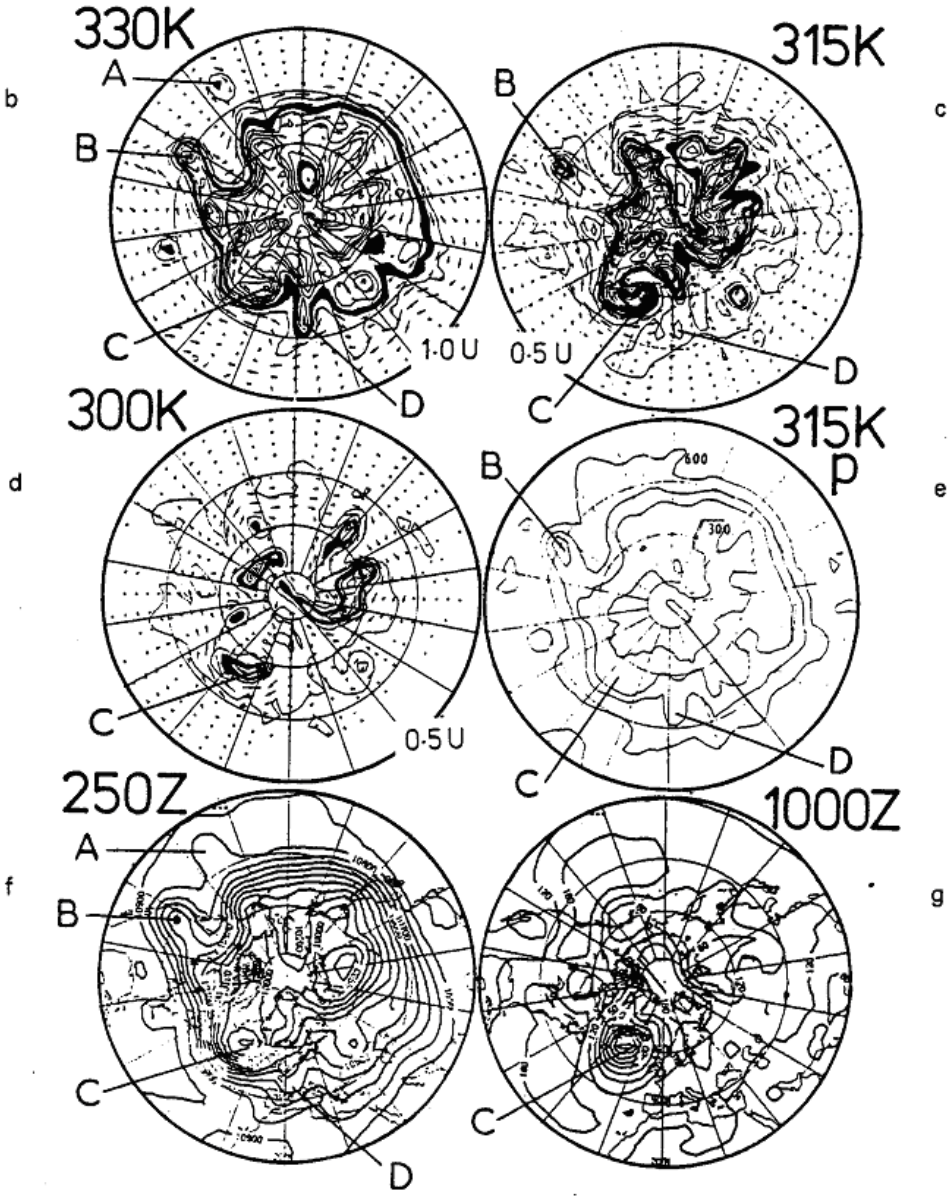

Figure 1.7: Northern Hemisphere synoptic fields for the 30 September 1982. Shown in (b), (c), and (d) are the PV maps on the 330 K, 315 K and 300 K isentropic surfaces, respectively. As indicated, the contour intervals are 1.0, 0.5 and 0.5 PVU, respectively. The values 2-3 units in (b) and 1.5-2 units in (c) and (d) have been blacked in. Wind vectors are as in Fig. 1.6, but unlike in Fig. 1.6, the boundary circle is 20^oN. The contours in (e) are of the pressure p on the 315 K surface, the contour interval being 100 mb. The 250 mb and 1000 mb geopotential height fields are shown in (f) and (g), with contour intervals of 100 m and 60 m respectively. (from HMR)

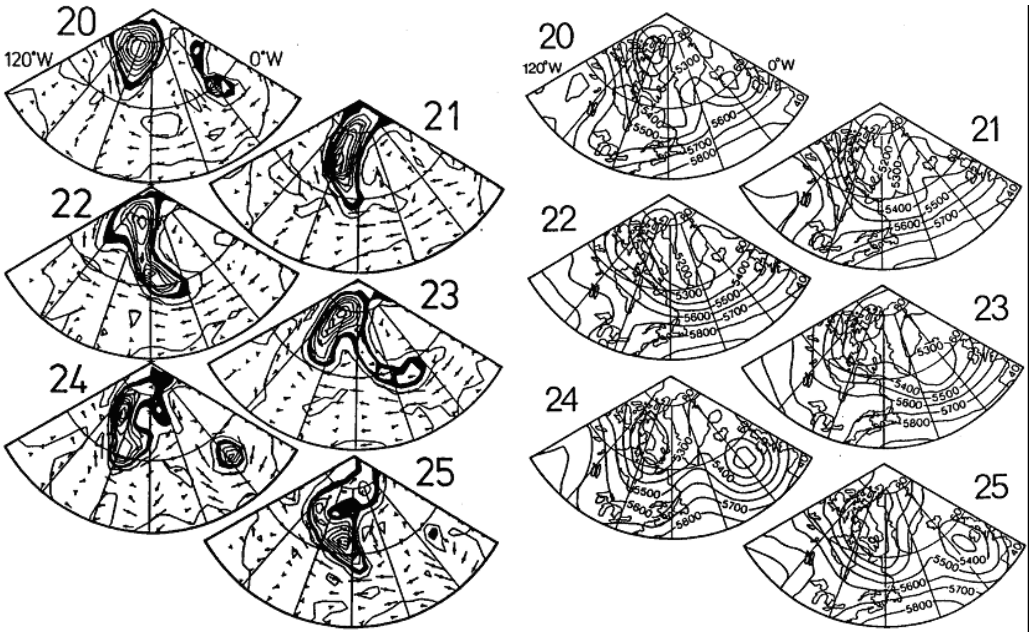

Figure 1.8: (a) Sectors of the 300 K PV maps for the period 20-25 September 1982. The region covered is from 40°N to the north pole and from 120°W to 0°W with the 60°W meridian central. The contour interval is 0.5 PV units and the region 1.5-2 units is blacked in. Also shown are the horizontal velocity vectors on this surface, as scaled in Fig. 1.5. (b) The 500 mb geopotential heights corresponding to the PV maps shown in (a). The contour interval is 100 m. (From HMR)

Feature C corresponds with a trough that extends through the whole depth of the troposphere while, trough *D* is mainly an upper level feature.

HML (Figs. 1.3 and 1.4) show time sequences of PV charts to illustrate the evolution of various types of systems and they compare the PV evolution with the evolution in the geopotential height fields on selected isentropic surfaces. They show also an example of the formation of a cutoff low, illustrated here in Fig. 1.8a.

In this an upper-air anomaly, consisting of high-PV stratospheric air, was advected near Hudson Strait across the Atlantic towards Europe, and appeared to roll itself up into a large cutoff cyclone (at 18°W on 24 Sept.). Fig. 1.8b shows the 500 mb geopotential heights corresponding to these PV maps, while Fig. 1.9 shows the 1000 mb geopotential and 700 mb temperature fields for the period 22-24 September covering the period of cutoff. This is an example of the simplest kind of cyclogenesis when a single upper-air PV

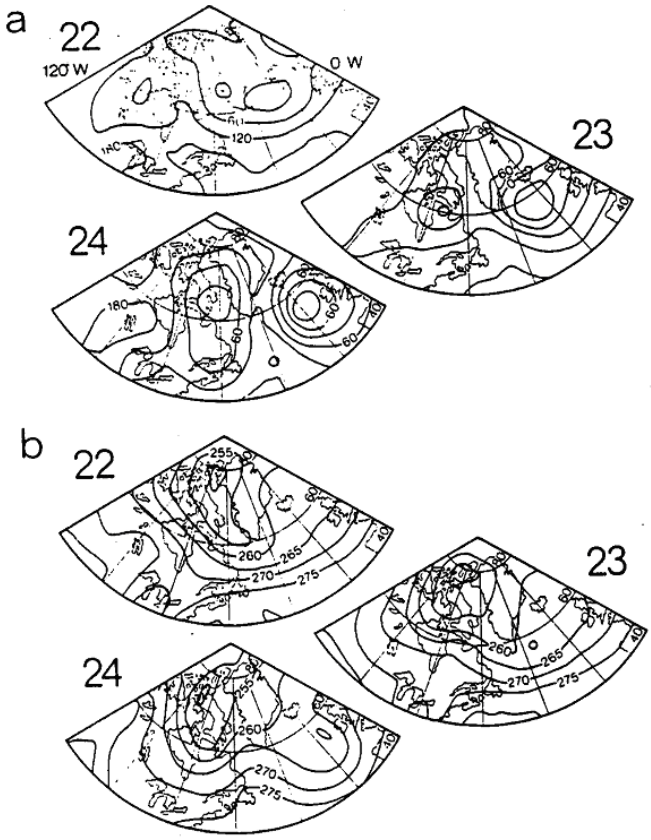

Figure 1.9: The 1000 mb geopotential (a) and 700 mb temperature (b) for the period 22-24 September 1982 and the region 40°N - 90°N and 120°W-0°W corresponding to that shown in Fig. 1.8. The contour intervals are 60 m and 5 K, respectively. (from HMR)

anomaly is advected into a region from a location where its surroundings made it less "anomalous" (McIntyre, 1988a). We are led to enquire into the typical vertical structure of such anomalies. An indication of what to expect is provided by some calculations by Thorpe (1985, 1986).

1.4.2 The vertical structure of upper-air PV anomalies

Figure 1.10 shows the vertical structure of disturbances associated with axisymmetric upper-air potential vorticity anomalies. These diagrams are based on numerical solutions of the inversion problem for EPV, assuming the disturbances to be in gradient wind balance. A positive anomaly located near

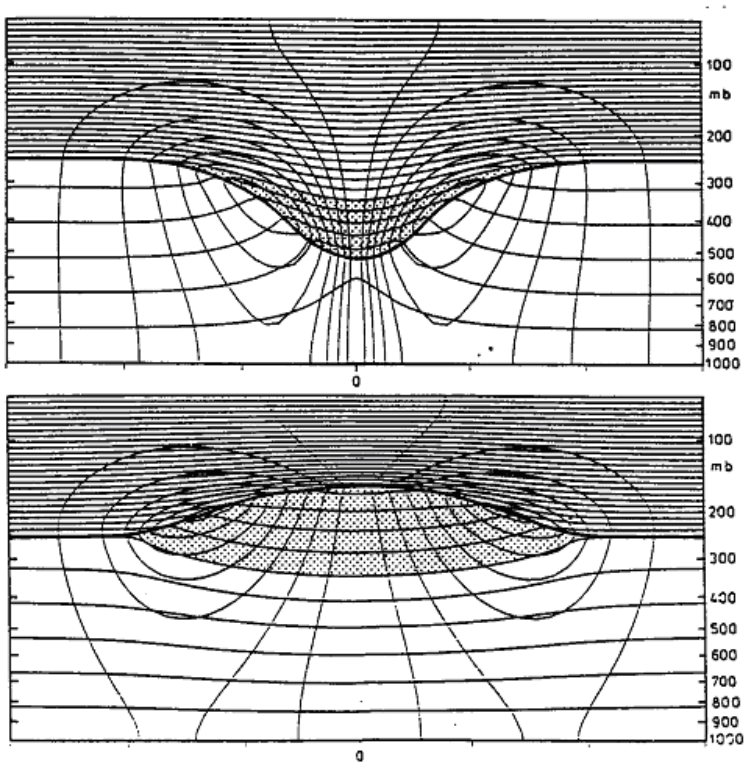

Figure 1.10: Circularly symmetric flows induced by simple, isolated, upper-level PV anomalies (location stippled). The quasi-horizontal lines are the isentropes while the thinner lines are the isotachs. The thick line represents the tropopause. Further details are given in HMR (see caption to Fig. 15.)

the tropopause (Fig. 1.10a) has a cyclonic circulation associated with it while a negative anomaly (Fig. 1.10b) has an anticyclonic circulation. The circulation is most intense at the level of the anomaly and decays with height above and below the anomaly. The isentropes show a characteristic pattern also. For a positive anomaly, they are raised below the anomaly, indicating reduced static stability and are lowered above, a feature reflected in the lowered tropopause in the vicinity of the anomaly. For a negative (anticyclonic) anomaly these features are reversed; there is enhanced static stability below the anomaly and the tropopause is raised above the anomaly. Such structures are quire realistic; for example Fig. 1.11 shows the analogous isentrope structure through a cutoff low in an early observational analysis of Peltonen (1963). In a stationary anomaly, there is no vertical motion.

An important feature of these structures is that they are carried along

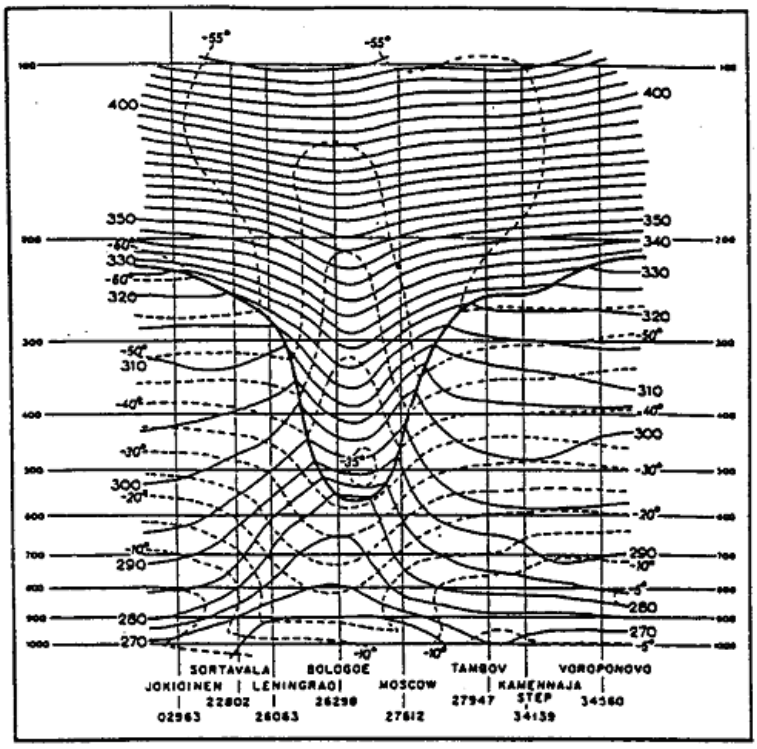

Figure 1.11: A vertical section through a cutoff cyclone at 12 GCT November 16 1959 produced by Peltonen (1963). The heavy line represents the tropopause; dashed lines are isotherms at 50°C intervals and solid lines isentropes every 5 K. The centre of the cyclone was at about 350°E, 58°N. (from HMR)

with an anomaly if it moves. This implies the existence of a pattern of vertical motion. For example, as a positive anomaly advances, air below and ahead of it must ascend along the raised isentropes, while air behind it descends along the isentropes. The reverse is true for a moving negative anomaly. In reality, these patterns of vertical motion can be expected to relate to observed areas of cloudiness or of cloudless skies in systems. In the next chapter we shall go on to examine other types of cyclogenesis events in a PV framework.

Chapter 2

A Potential Vorticity view of cyclogenesis

2.1 Preliminary Ideas

In the previous chapter we examined one very basic type of cyclogenesis leading to the formation of a cutoff low. However, this is not the only kind and is not associated with baroclinic energy conversions. How then are such energy conversions manifest in a PV description? The answer to this problem has its origins in a paper by Bretherton (1966) and was further refined by McIntyre (early '70's, unpublished lecture notes). Bretherton showed that *temperature gradients at boundaries characterizing low-level baroclinic zones are mathematically equivalent to thin layers of potential vorticity just above the boundary with horizontal gradient proportional to the temperature gradient.* In particular, isolated temperature anomalies at a boundary are equivalent to potential vorticity anomalies of the appropriate sign. This revolutionary idea makes it possible to present a unified picture of the baroclinic instability mechanism in terms of PV and it allows us also to do the same for cyclogenesis. Because of the importance of the result I shall try to sketch out how it comes about by way of a simple calculation.

2.2 Surface layers of PV

I would like to show how a horizontal temperature gradient at the surface can be regarded as equivalent to a thin layer (or "sheet") of PV at the surface. In fact, I shall demonstrate this result for the case of PV in a quasi-geostrophic flow.

Consider a zonal flow with uniform vertical shear $u = U'z$ (U' constant)

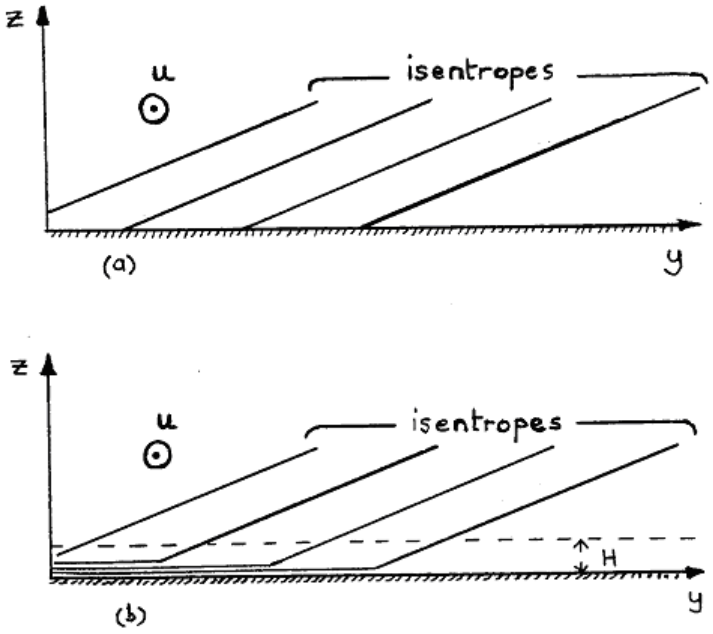

Figure 2.1: (a) Sloping isentropes in a uniform zonal shear flow $u = U'z$ (U' a positive constant) assuming gradient wind balance, $fU' = -(g/\overline{\theta})(\partial\theta/\partial y)$. (b) Analogous situation when the isentropes turn to become horizontal in a thin layer above the surface. This surface layer is equivalent to a layer of PPV gradient $\partial\overline{q}_{avr}/\partial y$, as discussed in the text.

in thermal wind balance with a uniform meridional potential temperature gradient $\partial\theta/\partial y$. Mathematically, thermal wind balance implies that

$$f\frac{\partial u}{\partial z} = -\frac{g}{\overline{\theta}}\frac{\partial\theta}{\partial y}, \tag{2.1}$$

where $\overline{\theta}$ is some reference potential temperature. The geostrophic streamfunction satisfying Eq. 1.2 is

$$\psi = -U'yz \tag{2.2}$$

so that for $z > 0$, $q = 0$ (refer to Eq. 1.8). The isentropes and flow configuration are sketched in Fig. 2.1a.

Imagine now a similar flow configuration in which the sloping isentropes become horizontal in a shallow surface-based layer of depth H (Fig. 2.1b). Now there is no surface gradient of potential temperature. The average q in this layer can be estimated by integrating Eq. 1.8 through the layer, i.e.,

$$\overline{q}_{avr} \equiv \nabla_h^2 \psi_{avr} + \frac{\varepsilon^2}{H}\left[\left.\frac{\partial\psi}{\partial z}\right|_{z=H} - \left.\frac{\partial\psi}{\partial z}\right|_{z=0}\right] \tag{2.3}$$

Now, we let $H \to 0$ so that the surface layer becomes infinitely thin. Then $\psi_{avr} \to \psi(0) = 0$, using Eq. 2.2. We assume further that $\partial\psi/\partial z = 0$ at $z = 0$. Then using (2.2), (2.3) becomes

$$q_{avr} = \frac{\varepsilon^2}{H}\left.\frac{\partial\psi}{\partial z}\right|_{z=H} = -\frac{f^2 U'}{N^2 H} y, \tag{2.4}$$

and using (2.1),

$$\partial q_{avr}/\partial y = \left[gf/(N^2 H\overline{\theta})\right](\partial\theta/\partial y)\,. \tag{2.5}$$

We have shown that the presence of a surface potential temperature gradient at a boundary is mathematically equivalent to a flow with no such gradient, but with a thin layer of potential vorticity adjacent to the boundary, provided we choose $\partial\psi/\partial z = 0$ as the boundary condition on ψ at the boundary. Moreover, the horizontal gradient of potential vorticity in this layer is proportional to the horizontal temperature gradient above the layer (Eq. 2.5)[1]. Although demonstrated in a simple case, it is a general result that horizontal temperature gradients at boundaries are equivalent to horizontal gradients of potential vorticity there.

Analogous to Fig. 1.11, Fig. 2.2 shows the vertical structure of axisymmetric flows associated with isolated surface temperature anomalies, or equivalently with isolated surface PV anomalies (in this case EPV). The calculations were again carried out by Thorpe (1985) assuming gradient wind balance. Characteristically, a warm surface anomaly is associated with isentropes that dip down above the anomaly and with a cyclonic wind circulation that decays with height (Fig. 2.2a). In contrast, a cold anomaly has isentropes that bulge upwards and an anticyclonic circulation (Fig. 2.2b).

2.3 Potential vorticity gradient waves

In chapter 1 I discussed the dynamics of a barotropic Rossby wave in a β-plane channel. These ideas generalize readily to quasi-geostrophic wave motions in a stably-stratified rotating fluid governed by Eqs. (1.7) and (1.8). Let us consider the case where there is a basic state meridional gradient of

[1] In the limiting case as $H \to 0$, the layer becomes a sheet of infinitesimal thickness. Mathematically, $\partial q_{avr}/\partial y$ is then expressed in terms of the Dirac Delta function.

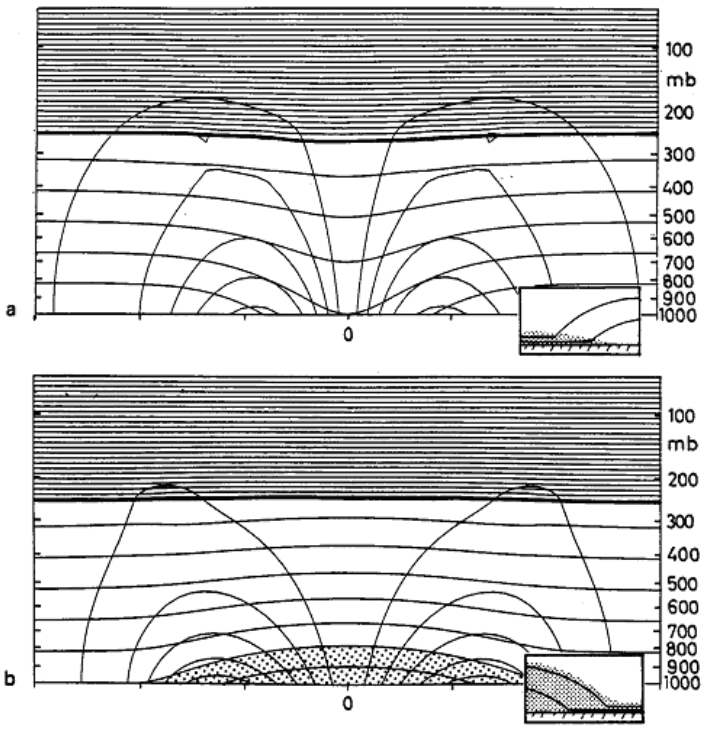

Figure 2.2: Circularly symmetric flows induced by simple boundary temperature anomalies. Otherwise similar to Fig. 1.10. The warm anomaly (a) induces a cyclonic circulation, and the cold anomaly (b) an anticyclonic circulation. The insets and stippling suggest the interpretation of the warm surface potential temperature anomaly as equivalent to a cyclonic PV anomaly, and the cold surface potential temperature anomaly as part of an anticyclonic PV anomaly. (from HMR)

PPV, $\overline{q}_y$, in some region. Away from horizontal boundaries, this is related to the basic state zonal flow $\overline{u}(y,z)$ by

$$\overline{q}_y = \beta - \frac{\partial^2 \overline{u}}{\partial y^2} - \frac{\partial^2 \overline{u}}{\partial z^2}, \tag{2.6}$$

obtained by differentiating Eq.(1.8) with respect to y and remembering that $\overline{u} = -\partial\overline{\psi}/\partial y$. At a horizontal boundary where there is a meridional temperature gradient, there is an additional contribution to $\overline{q}_y$ in a thin sheet at the boundary given by (2.5).

Writing $q = \overline{q} + q'$ in (1.7) and assuming the perturbation PPV, q', to be of sufficiently small amplitude, we can linearize (1.7) to obtain

$$\frac{\partial q'}{\partial t} + \overline{u}\frac{\partial q'}{\partial x} + v\frac{\partial \overline{q}}{\partial y} = 0. \tag{2.7}$$

Moreover, using (1.8), q' is related to the geostrophic streamfunction perturbation ψ' by

$$\nabla_h^2 \psi' + \varepsilon \frac{\partial^2 \psi'}{\partial z^2} = q' \tag{2.8}$$

A simple case is when the zonal flow is a linear function of height, say $\overline{u} = U'\,z$, where U' is a constant. Then $\overline{q}_y = \beta$ from (2.6) and has uniform layer distributions $-f^2U'/(N^2H)$ at $z = 0$ according to (2.4) and $-f^2U'/(N^2H)$ at $z = H$, obtained in an analogous manner to (2.4). In some situations these layer distributions may be more important than the interior distribution associated with β.

As in the Rossby wave example studied earlier, there exist perturbation wave solutions, independent of y and travelling in the x-direction. However, the perturbations now have structure in the z-direction also. Even so, the earlier line of argument can still be used with effect.

We saw in chapter 1 that the largest meridional gradients of PV in the atmosphere occur near the tropopause. Significant gradients may occur also near the surface, in so-called "baroclinic zones" where there are relatively large horizontal temperature gradients. I am thinking here of synoptic-scale gradients rather than gradients at fronts. These observations lead us to consider wave propagation on layers of PV gradient, or more precisely in thin layers adjacent to boundaries, or PV sheets. In our case they are sheets of PPV, but from now on we shall drop the first 'P' because the ideas can be extended to EPV defined in (1.10) or (1.11).

Figure 2.3 shows the structure of a sinusoidal wave propagating along a sheet of PV gradient at an elevated boundary. We can think of this as a crude representation of the large PV gradient at the tropopause. If the

tropopause is thought of as a rigid lid above the uniform zonal shear flow $\overline{u} = U'\,z$, there will be a uniform meridional PV gradient in a sheet at the lid, associated with a uniform potential temperature gradient there. Both of these gradients are positive. For the present we neglect the earth's vorticity gradient characterized by β.

As in the Rossby wave example we suppose that the disturbance is such, that material surfaces, initially in $x - z$ planes, are deformed into sinusoidal corrugations that are independent of height. This will lead to PV perturbations *in the sheet*, exactly as in example 3.3, but not elsewhere These are associated with streamfunction perturbations governed by (2.8) which, because the disturbance is independent of y, takes the form

$$\overline{u} = U'\,z. \tag{2.9}$$

The membrane analogy can again be used again to infer the pattern of ψ' corresponding with that of q', but, first we must rescale z, defining $Z = \varepsilon^{\frac{1}{2}}\,z$ so that both coefficients in Eq. (2.8) are unity. We think of $\psi'(x, Z)$ as the displacement of a semi-infinite membrane in which a sinusoidal force distribution $-q'$ is applied along its top edge[2]. Where q' is negative (anticyclonic in the Northern Hemisphere), ψ' is positive and where q' is positive (cyclonic), ψ' is negative. Contours of ψ' in the $x - z$ plane are included also in Fig. 2.3. Remember that ψ' is proportional to the pressure perturbation in the disturbance. There are two features particularly worthy of note:

1. Although the "forcing" is *at the boundary*, the response extends a certain distance below the boundary with penetration scale D.

2. In the rescaled domain (x, Z), the equation for ψ' corresponds with that for an isotropic membrane, i.e., one is displaced equally in all directions in response to a localized point force. This means that the vertical scale of the disturbance is comparable with the horizontal scale L. Therefore, making the reverse transformation, the penetration scale in physical space $D \sim L/\varepsilon^{\frac{1}{2}} = f\,L/N$ is for a given horizontal scale L. This is commonly referred to as the *Rossby height scale*.

The meridional velocity perturbation $v'(= \partial\psi'/\partial x)$ is indicated by arrows at points along the x-axis in Fig. 2.3. Note that v' is zero where particle

[2]Actually we must be careful about boundary conditions in this case. Inclusion of the PV-sheet just below $z = H$ allows us to set the meridional temperature gradient to zero at $z = H$ itself. This is equivalent to taking the boundary condition $\partial\psi'/\partial z = 0$ at $z = 0$, or to assuming that the membrane surface has zero slope at this boundary.

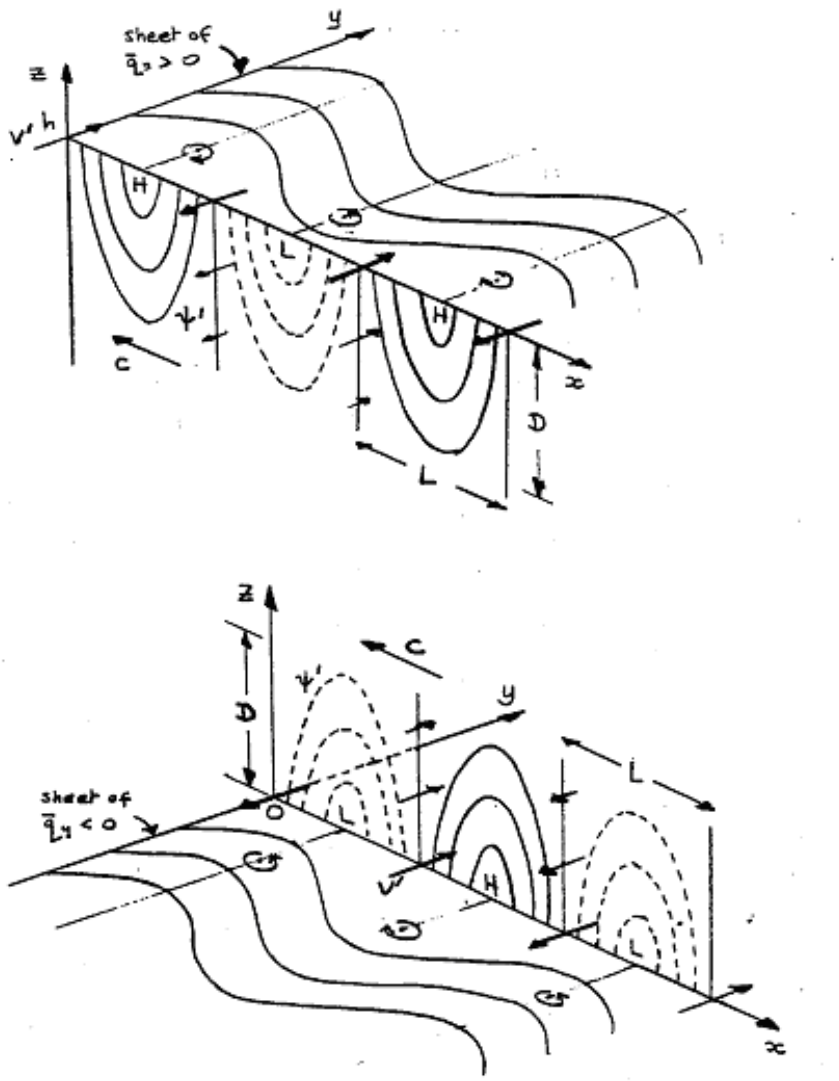

Figure 2.3: Diagram illustrating the structure of sinusoidal wave perturbations associated with sheets of potential vorticity at horizontal boundaries. (a) shows the structure of a wave on a PV-sheet with positive meridional gradient at an upper boundary. (b) shows the corresponding structure for a sheet with negative gradient at the lower boundary.

displacements are a maximum from equilibrium, and is a maximum to the west of the maximum poleward displacement of particles. Hence, just like the Rossby waves in example 3.3, the waves do not grow in amplitude with time and they propagate westward relative to the basic current at $z = H$.

If the tropopause is regarded as a deformable surface separating more stable stratospheric air ($N = N_1$) from less stable tropospheric air ($N = N_2$), the disturbance structure in the stratosphere will be a mirror image of that in the troposphere, but with a smaller depth scale $D_1 = (N_2/N_1)D_2$.

Figure 2.3b shows the analogous situation to Fig. 2.3a, but for waves on a sheet of negative PV gradient at the lower boundary, corresponding with the negative meridional temperature gradient there. Now the PV perturbations are restricted to the surface, but the corresponding streamfunction perturbations extend to the flow interior, again with the penetration scale fL/N. Again the waves are non-growing, but because the PV gradient is negative at the surface, the waves propagate eastward relative to the basic surface current (in the present example $\overline{u}(0) = 0$).

The addition of a uniform flow to either of the above configurations leads to an advective component of the wave motion with the same speed. Thus the sense of phase propagation indicated above is relative to the basic flow at the level of the PV sheet.

With these elementary concepts we are now in a position to discuss other types of cyclogenesis including the mechanism of baroclinic instability in terms of PV arguments.

2.4 Baroclinic Instability

In order to understand other mechanisms for cyclogenesis, it is insightful to examine the baroclinic instability problem which considers the growth of incipient disturbances in a baroclinic current. One of the simplest problems is that formulated by Eady (1949) who considered the stability of a uniform zonal shear flow $U = U'z$ to quasi-geostrophic wave perturbations. The β-effect was ignored, i.e. the calculations assumed a constant Coriolis parameter, and the flow was assumed to be confined between horizontal boundaries at $z = 0$ and $z = H$. The meridional (P)PV-gradient in the flow interior is then zero from Eq. (2.6), but there are sheets of PV at the boundaries, with negative meridional gradient at $z = 0$ and positive gradient at $z = H$. Accordingly we can think of possible disturbances as being composed of "potential vorticity gradient waves", for want of a better term, of the type outlined in Fig. 2.3. Indeed, I want to show that the unstable

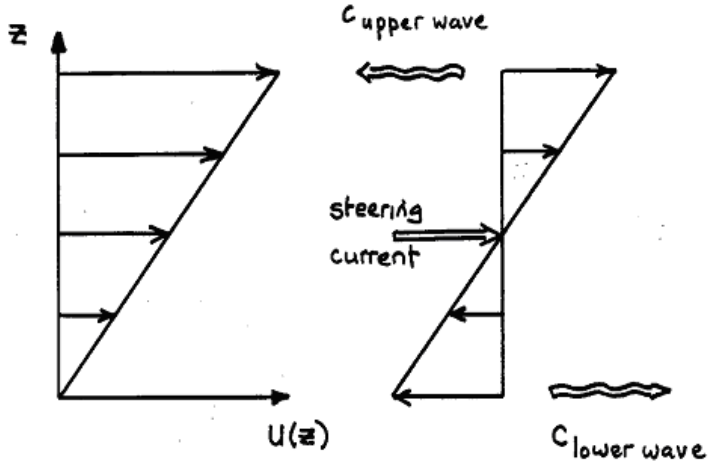

Figure 2.4: Steering current and relative flow in a uniform tonal shear flow showing the sense of relative advection at $z = 0$ and H and that of PV-gradient wave propagation (curly arrows) at these boundaries.

waves in the Eady problem can be understood in terms of two[3] sinusoidal waves of the same wavelength, one associated with the PV gradient at the upper boundary as in Fig. 2.3a, the other associated with the PV gradient at the lower boundary as in Fig. 2.3b.

A well-known result is that the unstable Eady waves propagate at the speed of the flow in mid-channel, $u = \frac{1}{2}U'H$, the "steering level" for these waves. This is consistent with the "steering principle" used as a rule of thumb in forecasting practice that deep tropospheric disturbances tend to move with the 500 mb flow. Now, relative to the steering flow, the upper wave propagates westwards, but is advected eastwards by the current- In contrast, the lower wave propagates eastwards, but is advected westwards relative to the steering flow (Fig. 2.4). The net speed and direction of each wave depends on the wavelength λ. As in the case of Rossby waves[4], propagation wins over advection if the wavelength is longer than a certain value, otherwise advection wins, but there is a wavelength at which the waves are both stationary in the frame of reference moving with the steering speed.

Consider a situation when the two waves are out-of-phase, e.g. suppose the upper low is westward of the surface low. Then provided the disturbance associated with each wave overlaps with that of the other, i.e. provided

[3]Remember that the problem is linear so that particular solutions can be superposed.

[4]The phase speed for Rossby waves on a uniform current U is $c_p = U - \beta\lambda^2/4\pi$.

$D \geq H$, then the meridional velocity perturbation of the upper wave is positive at the position in the lower wave where the meridional displacement of that wave is a maximum and vice versa. That means that each component wave will help to increase the meridional displacements of the other, and hence the amplitude of the other. With this phase configuration both waves will grow together in time. Note that this phase configuration is exactly the one you know from forecasting experience to be conducive to continued cyclogenesis in the atmosphere - one of the predictions, indeed, of Sutcliffe's theory!

If the phase is reversed, i.e. if the upper low is eastward of the lower one, the meridional velocity perturbation of the upper wave is negative at the position in the lower wave where the meridional displacement is a maximum. In this case the waves help each other to decay. This is exactly the structure of decaying modes in the Eady problem.

When the phase of the upper and lower waves is the same, i.e. when the upper low is exactly above that at the surface, the meridional velocity perturbation of each waves is zero where the meridional displacement of the other is an extremum, and like the Rossby wave, no growth occurs. This is exactly the structure of neutrally stable solutions to the Eady problem. Interestingly, it corresponds also with a result of forecasting experience: *when the surface low lies beneath the upper trough, further deepening of the low is not to be expected*. This is also a result of Sutcliffe's theory.

To answer the question as to how two such waves end up in a particular phase configuration we must turn to the initial value problem and consider how an arbitrary initial disturbance can be decomposed in terms of the elementary sinusoidal modes about which I have been talking. Time does not allow me to pursue this question. Nor do I have time to present an elegant argument as to why two waves, when once in phase, remain "locked-in-phase" as they grow. Accordingly, I refer you to McIntyre (l9SSb, §9). However, we have now developed the building blocks to understand other types of cyclogenesis to the one I described in chapter 1.

2.5 Applications to understanding cyclogenesis

At the end of chapter 1, I described one very simple mechanism for cyclogenesis which does not involve the baroclinic instability process. Baroclinic instability as described above may be responsible for the growth of some cyclones from incipient disturbances to a baroclinic shear flow, but this is

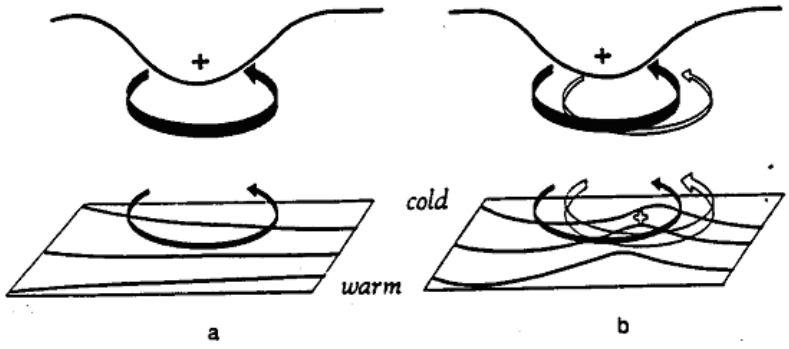

Figure 2.5: A schematic picture of cyclogenesis with the arrival of an upper-air PV anomaly over a low level baroclinic zone. (after HML)

difficult to establish because we cannot observe the incipient disturbance. It seems in the majority of cases, cyclogenesis takes place in the presence of finite amplitude perturbations. However, the ideas we have just described can be extended to this more realistic case.

Based again on results that go back to Sutcliffe (1947), synopticians pay attention to the presence of a "short wave" or "short-wave trough" on upper air charts. In PV terms, these are associated with cyclonic PV anomalies, usually around the tropopause level. Examples were shown in Figs. 1.6 and 1.7. They can be expected to have a similar vertical structure to that shown in Figs. 1.10-1.11.

HMR discuss what happens when an upper-air PV anomaly is advected over a low-level baroclinic region as shown in Fig. 2.5.

It is supposed in (a) that the anomaly, indicated by a solid plus sign and associated with the low tropopause shown, has just arrived over a region of significant low-level baroclinicity. The circulation induced by the anomaly is indicated by solid arrows, and potential temperature contours are shown on the ground. The low-level circulation is shown above the ground for clarity. The advection by this circulation leads to a warm temperature anomaly to the east of the upper PV anomaly as indicated in (b), and marked with an open plus sign[5]. This warm anomaly induces the cyclonic circulation indicated by the open arrows in (b). If the equatorward motion at upper levels advects high PV polar lower-stratospheric air, and the poleward motion advects low

[5]The structure of the low-level PV anomaly, associated with the surface temperature anomaly, becomes clearer when a suitable zonal average of the temperature field is removed. An example is given by Davis and Emanuel (1991, Fig. 6

PV sub-tropical upper tropospheric air[6], then the action of the upper-level circulation induced by the surface PV anomaly will, in effect, reinforce the upper-air PV anomaly. It will also slow down its eastward propagation as discussed by McIntyre (1988b).

(i) The degree of cyclogenesis will depend on a number of factors.

(ii) The strength of the upper-air PV anomaly.

(iii) The Rossby depth scale, $D = fL/N$, in relation to the altitude of this anomaly above the surface. Here H is the horizontal length scale of the anomaly.

(iv) The strength of the low-level anomaly, which will depend *inter alia* on the amount of low-level warm advection, and

(v) The extent to which phase-locking and mutual amplification of the surface and upper-air anomalies is significant.

The last three factors are all profoundly affected by latent heat release which *inter alia* affects the static stability N and hence the vertical penetration of the two separate PV anomalies.

In connection with (iv), it may not be the case that the upper and lower disturbances remain in phase for long enough for the development to correspond closely with the baroclinic wave mechanism described earlier. However, even a temporary interaction of the two disturbances may lead to a degree of cyclogenesis of significant interest to the forecaster.

In the example described above, it was assumed that both upper and lower anomalies were embedded in an environment with a large-scale PV-gradient. If this is not the case, the baroclinic instability mechanism cannot operate. However as one anomaly passes over the other, there will be a temporary reinforcement of each during the period that they are in phase and this may lead also to a cyclogenetic event of significance to the forecaster.

Some interesting three-dimensional depictions of the interaction between upper and lower PV anomalies associated with extratropical cyclogenesis are contained in a paper by Bleck (1990).

[6]This requires that the upper-air anomaly lie within an environment with large-scale meridional PV gradient.

Chapter 3

Invertibility, iso-PV charts, diabatic and frictional effects.

3.1 Invertibility of EPV

In the last lecture I discussed an extension of ideas based on quasi-geostrophic dynamics to real cyclones where the quasi-geostrophic approximation may be rather inaccurate. In atmospheric applications it is preferable to work with EPV instead of PV as it is conserved under more general conditions. Unfortunately, unlike PPV, EPV cannot be inverted to diagnose the flow associated with EPV anomalies, unless we make some assumption of balance. Geostrophic balance may not be sufficiently accurate for quantitative analysis, but there are other possibilities available. It is inappropriate here to go into details and I refer you to HMR and to Davis (1992) for a rather complete discussion and to Davis and Emanuel (1991) for an example. For qualitative insights, one can get a long way by assuming quasi-geostrophic balance.

3.2 Iso-PV charts

In Lecture 1 we saw that for adiabatic frictionless motion, P is materially conserved, i.e. conserved following an air parcel. But θ is materially conserved also, so that not only is P conserved on an isentropic surface, q is conserved on an iso-P surface. In particular, θ is conserved on the $P = 2PVU$ surface which, as noted earlier, coincides closely with the tropopause in extra-tropical latitudes. We have seen that quasi-horizontal PV-gradients tend to be large in the vicinity of the tropopause so that this level is one of particular interest *vis-á-vis* upper-level PV anomalies. We have seen also (albeit in a

quasi-geostrophic framework) that horizontal PV gradients are analogous to horizontal temperature gradients. Therefore, instead of plotting a whole lot of PV-chart on isentropic surfaces, it may be sufficient to have one iso-PV = 2 chart of selected isentropes. While is PV = 2 charts and PV-charts show similar features, the former have the added a advantage that inspection of the θ-values gives an idea of the height of the tropopause, i.e., the tropopause "topography". Such charts could be used in conjunction with a low-level chart indicating low-level baroclinicity, such as potential temperature at 850 mb. An example is given by Hoskins and Berrisford (1988).

3.3 Diabatic and frictional effects

When diabatic and/or frictional effects are present, PV is no longer materially conserved, but is governed by the equation

$$\frac{DP}{Dt} = \frac{1}{\rho}\zeta_a \cdot \nabla\dot{\theta} + \frac{1}{\rho}\mathbf{K} \cdot \nabla\theta = \frac{1}{\rho}\nabla \cdot \mathbf{Y}, \tag{3.1}$$

where ζ_a is the *absolute vorticity*, $\dot{\theta}$ is the diabatic heating rate, $\mathbf{K}$ represents the curl of the frictional force $\mathbf{F}$ per unit mass (i.e. $\mathbf{K} = \nabla \cdot \mathbf{F}$) and

$$\mathbf{Y} = -\dot{\theta}\zeta_a + \nabla\theta \wedge \mathbf{F}. \tag{3.2}$$

When integrated over a region of space V, Eq.(3.1) gives

$$\frac{d}{dt}\int_V \rho P dV = \int_S (\dot{\theta}\zeta_a + \theta\mathbf{K}) \cdot \hat{\mathbf{n}} dS, \tag{3.3}$$

where S is the surface of V and $\hat{\mathbf{n}}$ is the unit normal to S, outward from V.

An important result that follows from (3.3) is that purely internal diabatic heating or friction cannot change the mass-weighted PV distribution within V, i.e., if $\dot{\theta}$ and $\mathbf{K}$ are zero on S, then

$$\frac{d}{dt}\int_V \rho P dV = 0. \tag{3.4}$$

Thus internal diabatic heating or friction can only redistribute the PV that is there. Equation (3.2) shows that diabatic heating in a localized region produces a dipole anomaly of PV with its axis oriented along the absolute vorticity vector ζ_a and in the opposite direction to it (Fig. 3.1a). Cooling instead of heating reverses the direction of the dipole (Fig. 3.1b). An alternative interpretation of the effects of diabatic heating and cooling is given by Haynes and McIntyre (1987), based on the result that there can be no

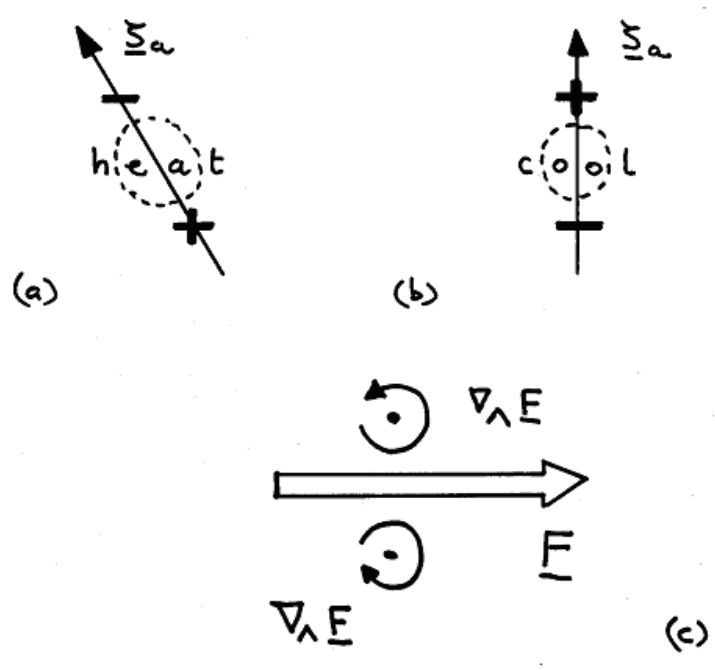

Figure 3.1: PV dipole produced by localized diabatlc heating (a), or cooling (b). (c) shows the force-curl dipole associated with a localized farce **F**.

transport of "PV-substance" across isentropic surfaces, even in the presence of diabatic effects (see also Haynes and McIntyre, 1990).

The action of a localized force **F** produces positive relative vorticity to its left and negative relative vorticity to its right (Fig. 3.1c), at a rate K equal to $\nabla \wedge \mathbf{F}$. Recalling that $P = (1/\rho)\zeta_a \cdot \nabla\theta$ and noting that the frictional generation term in (3.1) has the form $(1/\rho)\nabla \wedge \mathbf{F} \cdot \nabla\theta$, we see how the latter contributes to a change in and hence a change in $(1/\rho)\boldsymbol{\zeta}_a \cdot \nabla\theta$. Note that again, a localized force produces a dipole anomaly of PV, being the projection of the dipole anomaly of $\boldsymbol{\zeta}_a$, i.e. $\nabla\wedge\mathbf{F}$, on the potential temperature gradient, $\nabla\theta$. Consider the case of an axisymmetric vortex with tangential velocity distribution $v(r)$, and assume a linear frictional force $\mathbf{F} = -\mu v(r)$, $\mu(> 0)$ acts at the ground $z = 0$. Then $\mathbf{K} = -\mu\zeta\mathbf{k}$, where ζ is the vertical component of relative vorticity. Then PV is destroyed locally at the boundary at the rate $(1/\rho)(\mathbf{K} \cdot \nabla\theta) = -(1/\rho)\mu\zeta(\partial\theta/\partial z)_{z=0}$. The frictional force-curl term may be expected to be important in the boundary layer.

3.4 The effects of diabatic heating on cyclogenesis

Moist processes can greatly enhance surface development by reducing the effective static stability N. This increases the penetration depth D ($= fL/N$) of disturbances with a particular horizontal scale L. The result is to enhance the dynamical interaction between upper and lower level PV anomalies, leading to a more spectacular development. The enhanced interaction has the effect also of slowing down the relative motion of the upper anomaly to the lower one, i.e. it accentuates the degree of phase-locking (McIntyre, 1988b, §11). Latent heat release in the middle troposphere will tend also to lower the PV anomaly as suggested by Fig. 3.1a.

3.5 The demise of cutoff lows and blocking anticyclones

Consider a cutoff cyclone associated with an upper level PV anomaly of the type discussed in Lecture 1 (see Figs. 2.4 and 2.5). HMR point out that the area of reduced static stability below the anomaly (c/f Figs. 1.10a and 1.11) is a preferred one for deep convection to occur. Associated latent heat release will produce a PV dipole anomaly, negative aloft, tending to weaken the upper anomaly, and positive below, strengthening the anomaly at lower levels. In other words, the net effect of the convection is to move the cyclonic PV anomaly down to lower tropospheric levels. HMR argue that, in order to annihilate the cyclone completely, the diabatically-induced vertical redistribution of PV would have to extend all the way down to the surface, and be accompanied by the destruction of mass-integrated PV by surface friction as discussed in section 3.3. They show that latent heat release in deep tropospheric convection can lead to the efficient diabatic decay of an upper PV anomaly on a time scale of a few days.

A unifying aspect of 'PV thinking' is the conceptual duality it provides between cutoff lows and blocking highs. The latter are associated with anticyclonic upper-air anomalies of PV and have a vertical structure typified by Fig. 1.10b, i.e. a raised tropopause with depressed isentropes below the anomaly consistent with enhanced static stability there. However, there is no duality for their diabatic modification which tends to be much faster for cyclones than anticyclones. HMR point out that the crucial difference is the tropospheric static stability induced by the PV anomaly. This suppresses deep convection, leaving radiative cooling as the main diabatic process. This

gives a decay time scale of a week or so.

3.6 Advantage of PV analysis of cutoff lows

Meteorologists have traditionally considered the difference between "cutoff" and "non-cutoff" weather systems in terms of the existence or nonexistence of closed geopotential contours at middle and upper tropospheric levels. As noted by HMR, this distinction is unsatisfactory because it is not Galilean-invariant; i.e. if one adds a uniform translation speed to the whole system, its classification may change although the dynamics would not. In contrast, the PV structure *is* Galilean-invariant and should provide a better basis for distinguishing between cutoff and non-cutoff systems.

3.7 The PV structure of tropical cyclones

A key aspect of tropical cyclogenesis is the release of latent heat associated with vigorous deep convection. We have seen that such heating tends to produce a low-level cyclonic PV anomaly and an anticyclonic anomaly in the upper troposphere (Fig. 3.1a). In the case of a tropical cyclone, this distribution is subject to advection by the meridional circulation so that the low-level anomaly extends through much of the depth of the troposphere and the anticyclonic anomaly is spread in a wide, but shallow layer in the outflow layer, just below the tropopause. The way in which these structures evolve, is illustrated in a simple model calculation by Schubert and Alworth (1987). Figure 3.2 shows the results of a similar calculation by Möller and Smith (1994) in which a vortex is generated by switching on a fixed heat source in an annular region around the axis of rotation, a configuration that attempts crudely to represent the effect of latent heat release in the tropical cyclone's eye-wall clouds.

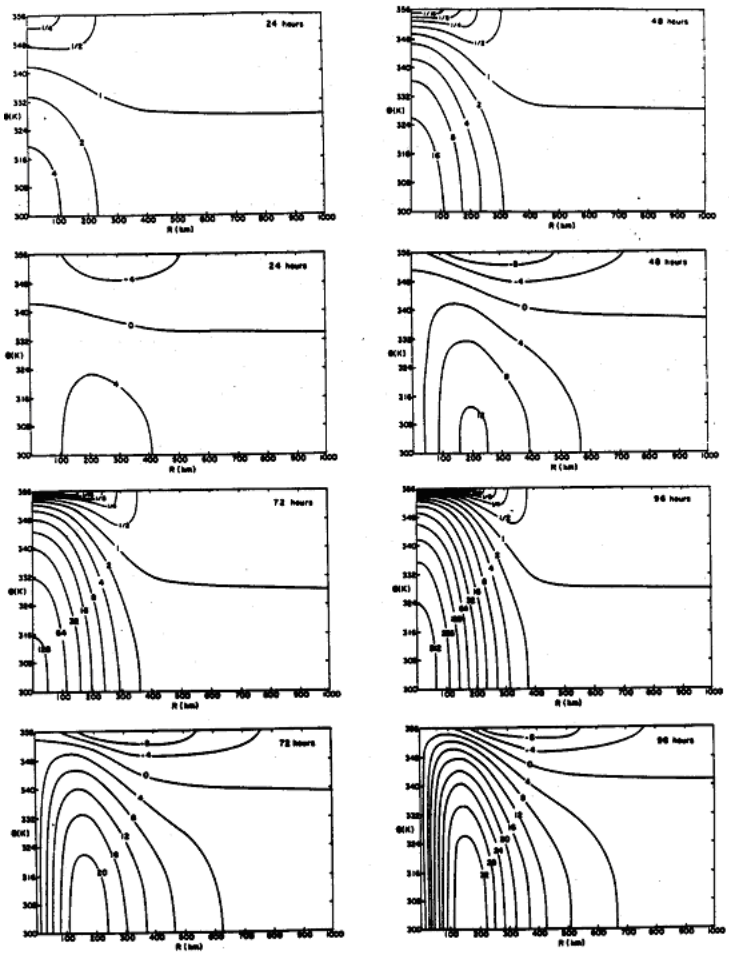

Figure 3.2: Isolines of the dimensionless PV(upper diagram and the tangential wind speed (lower diagrams) induced by a fixed symmetric heat source surrounding the axis of a uniformly rotating fluid. The heat source is imposed at the initial time and panels show the evolution of fields at 24 hour intervals. The calculation illustrates the evolution PV structure In a tropical cyclone. In these diagrams, Isentropic coordinates are used in the vertical and a stretched radial coordinate in the horizontal direction. (From Schubert and Alworth, 1987).

Bibliography

[1] Bleck, R., 1990: Depiction of upper/lower vortex interaction associated with extratropical cyclogenesis. *Math. Wea. Rev.*, **118**, 573-585.

[2] Bretherton, F. P., 1966: Critical layer instability in baroclinic flows. *Quart. J. Roy. Meteor. Soc.*, **92**, 325-334.

[3] Charney, J. G., 1947: The dynamics of long waves in a baroclinic westerly current. *J. Meteor.*, **4**, 135-163.

[4] Davis, C. A., 1992: Piecewise potential vorticity inversion; *J. Atmos. Sci.* **49**, 1397-1411.

[5] Davis, C. A., and K. A. Emanuel, 1991: Potential vorticity diagnostics of cyclogenesis. *Mon. Wea. Rev.*, **119**, 1929-1953.

[6] Eady, E. T., 1949: Long waves and cyclone waves. *Tellus*, **1**, 33-52.

[7] Haynes, P. H., and M. E. McIntyre, 1987: On the evolution of vorticity and potential vorticity in the presence of diabatic heating and frictional or other forces. *J. Atmos. Sci.*, **44**, 828-841.

[8] Haynes, P. H., and M. E. McIntyre, 1990: On the conservation and impermeability theorems for potential vorticity. *J. Atmos. Sci.*, **47**, 2021-2031.

[9] Hoskins, B. J., 1990. Theory of extratropical cyclones. Chapter 5 of Extratropical Cyclones: The Erik Palmen Memorial Volume, *Amer. Meteor. Soc.*, 63-80.

[10] Hoskins, B. J., M. E. McIntyre, and A. W. Robertson, 1985: On the use and significance of isentropic potential vorticity maps. *Quart. J. Roy. Meteor. Soc.*, **111**, 877-946. (See also **113**, 401-404, comments by J. S. A. Green and reply by authors.)

[11] Hoskins, B. J., and P. Berrisford, 1988: A potential vorticity perspective of the storm of 15-16 October 1987. *Weather*, **43**, 122-129.

[12] Möller, J. D., and R. K. Smith, 1994: The development of potential vorticity in a hurricane-like vortex. *Quart. J. Roy. Meteor. Soc.*, **120**, 1255-1265.

[13] McIntyre, M. E., 1988a: The dynamical significance of potential vorticity and low-level distributions of potential temperature. *Proceedings, The nature and prediction of extra-tropical weather systems. Vol 1.* European Centre for Medium Range Weather Forecasting, Reading, England, 237-259.

[14] McIntyre, M. E., 1988b: The use of potential vorticity and low-level temperature/moisture to understand extratropical cyclogenesis. *Ibid*, 261-280.

[15] Peltonen, T., 1963: A case study of an intense upper cyclone over eastern and northern Europe in November 1959. *Geophysica (Helsinki)*, **8**, 225-251.

[16] Schubert, W. H., and B. T. Alworth, 1987: Evolution of potential vorticity in tropical cyclones. *Quart. J. Roy. Meteor. Soc.*, **113**, 147-162.

[17] Smith, R. K. 1998: Lectures on Dynamical Meteorology. (unpublished notes, available from http://www.meteo.physik.uni-muenchen.de)

[18] Smith, R. K., and W. Ulrich, 1990: An analytical theory of tropical cyclone motion using a barotropic model. *J. Atmos. Set*, **47**, 1973-1986.

[19] Smith, R. K., W. Ulrich, and G. Dietachmayer, 1990: A numerical study of tropical cyclone motion using a barotropic model. I: The role of vortex asymmetries. *Quart. J. Roy. Meteor. Soc.*, **116**, 337-362.

[20] Sutcliffe, R. J., 1947: A contribution to the problem of development. *Quart. J. Roy. Meteor. Soc.*, **73**, 370-383.

[21] Thorpe, A. J., 1985: Diagnosis of balanced vortex structure using potential vorticity. *J. Atmos. Sci.*, **42**, 397-406.

[22] Thorpe, A.J., 1986: Synoptic scale disturbances with circular symmetry. *Mon. Wea. Rev.*, **114**, 1384-1389.